Available online at www.sciencedirect.com

ScienceDirect

Ceramics International 40 (2014) 1961–1970

CERAMICS INTERNATIONAL

www.elsevier.com/locate/ceramint

Use of bauxite from Cameroon for solid state sintering and characterization of calcium dialuminate ($CaO \cdot 2Al_2O_3$) refractory cement

A.B. Tchamba[a,c,d,*], U.C. Melo[a,d], G.L. Lecomte-Nana[c], E. Kamseu[d], C. Gault[c], R. Yongue[b], D. Njopwouo[a]

[a]Department of Inorganic Chemistry, Mineral Materials laboratory, University of Yaoundé I, P.O. Box 812, Yaoundé, Cameroon
[b]Department of Earth Science, University of Yaoundé 1, P.O. Box 812, Yaoundé, Cameroon
[c]Groupe d'Etude des Matériaux Hétérogènes, Centre Européen de la Céramique, 12 rue Atlantis, 87068 Limoges Cedex, France
[d]Laboratory of Materials, Local Materials Promotion Authority, P.O. Box 2396, Yaoundé, Cameroon

Received 3 May 2013; received in revised form 17 July 2013; accepted 17 July 2013
Available online 30 July 2013

Abstract

Well crystallized matrices of $CaO \cdot 2Al_2O_3$ were successfully sintered using three bauxites (BX3, BX55 and BX8) containing respectively 80.2; 89.4 and 91.1 wt% of Al_2O_3 and the appropriate amounts of lime. XRD data on the solid state sintered samples at 1550 °C show crystalline $CaO \cdot 2Al_2O_3$ as the major phase. The XRD pattern of the clinker made with BX3 showed relatively low intensities of $CaO \cdot 2Al_2O_3$ peaks compared with BX55 and BX8, together with CT and AT additional phases which were not identified in BX55 and BX8. This difference in composition was explained by the Al_2O_3 content and the high concentration of Fe_2O_3 (8.7 wt%) and TiO_2 (7.1 wt%) in BX3 and was correlated to the difference in densification (3.17 g/cm^3 for BX3 and 2.95 cm^3 for BX55 and BX8) and specific area (0.72 m^2/g for BX3 and 0.85 m^2/g for BX55 and BX8). The Young modulus increased from 35.5 GPa (BX3) to 39.4 GPa (BX55). Unlike the Al_2O_3 content, the variation of the Young modulus indicated that the reactions of sintering and densification conducting to $CaO \cdot 2Al_2O_3$ are sensitive to the iron and titanium content.

Keywords: Alumina; Refractory; Cement; Bauxite; Calcium dialuminate

1. Introduction

Refractory cements are associated with industrial development. Calcium aluminates have long been one of the most suitable and efficient refractory cement materials used in the steel industry and as hydraulic materials in many cement applications [1,2]. In recent years, there has been an increasing interest in the synthesis of monolithic refractory materials [1–4]. Some amorphous calcium aluminates are photosensitive and hence are potential candidates for optical information storage devices. The production of amorphous calcium aluminate based refractories via the chemical route is linked with high mechanical performance, low porosity and good densification. Solid state reactions conducted by mixing powders under high thermal pressure form their first products at the interface of the grains (grain boundaries) and as the reactions proceed the reactants diffuse through the product layer resulting in the formation of amorphous calcium aluminates. The easier completion of such reactions depends on the tiny particle sizes of the reacting powders, their high specific area, the nature of alumina phase and the mixing process. The final properties of the as-produced clinker can then be monitored by the choice of raw materials, the composition design and the technological processing of the powders before sintering [5,6]. The behavior of such refractories depends strongly on the nature of the intergranular or bonding phases formed. The term "high alumina cement" (HAC) came into use when this type of cement, containing 32–45% Al_2O_3, was introduced in the UK after World War 1 to distinguish it from Portland type cement

*Corresponding author at: Department of Inorganic Chemistry, Mineral Materials laboratory, University of Yaoundé I and Local Materials Promotion Authority, P.O. Box 2396, Yaoundé Cameroon. Tel.: +237 99 30 10 69/ +237 70 56 96 79.
E-mail address: attchamba@yahoo.fr (A.B. Tchamba).

0272-8842/$ - see front matter © 2013 Elsevier Ltd and Techna Group S.r.l. All rights reserved.
http://dx.doi.org/10.1016/j.ceramint.2013.07.105

Nomenclature

C	CaO	T	TiO_2
A	Al_2O_3	CA_2	$CaO \cdot 2Al_2O_3$
S	SiO_2	H	H_2O
F	Fe_2O_3	C_3AH_6	$3CaO \cdot Al_2O_3 \cdot 6H_2O$
		gehlenite	$SiO_2 \cdot 2CaO \cdot Al_2O_3$
		spinel	$MgO \cdot Al_2O_3$

which contains much less alumina. Subsequently many other aluminous cements have been developed with alumina contents between 50% and 90% [1,6] intended mainly for refractory purposes in the steel industry and as hydraulic material in the cement community. Crystalline calcium aluminates are used in high strength and high toughness ceramic polymer composite materials [1,6]. Calcium dialuminate exhibits very low thermal expansion and excellent thermal properties and is thus considered a desirable phase for refractory applications; it is resistant to certain chemicals such as sulfates, as well as to hot and humid conditions. Some researchers [3,6,12] have investigated synthetic routes for amorphous calcium dialuminate based cement powder production as well as its pure anhydrous phases. Most of them tried it through solid state sintering with multiple stages [2–4] while others tried mechano-chemical routes [2,6]. The conventional route gives products which increase in strength with time after mixing the powder with water. The second route gives high strength at an early stage that decreases progressively with time after mixing the powder with water [2–6]. But in almost all cases the strength remained high after 28 days and the preparation methods still require improvements in energy consumption. Large area alumina with high porosity results from dehydroxylation of bauxite at 800–900 °C. It is then possible to project a direct synthesis of CA_2 using bauxite as a solid precursor through solid state sintering. Therefore bauxite is viewed as a low cost raw material and the use of one stage sintering permits an important energy saving. In tropical areas such as Cameroon, raw bauxite is characterized by the presence of some impurities such as iron and titanium based minerals. Hence, it is important to investigate the effect of these impurity phases on the sintering behavior and the final characteristics of the final calcium aluminate cements. (This paper presents studies on the synthesis of high alumina content (CA_2) refractory clinker powder using a one stage heating solid state sintering. The authors have used a single firing routine at 1500 °C on technical raw bauxite samples to prepare CA_2 with few low level traces of CA.). This demonstrates that, although previous successful preparations of CA_2 (from literature) required multiple high temperature firing or mechano-chemical treatment, it is possible to sinter it directly in one stage at high temperature by solid state sintering.

The production of CA_2 based cement aims at improving the resistance to chemical attack, to abrasion or impact and durability of the cement. Due to the high alumina content in the CA_2, its introduction into the cement matrix helps improve durability and stability of the cement in a concrete. The influence of impurities like TiO_2 and Fe_2O_3 contained in natural bauxite is elucidated in comparison with pure Bauxite samples.

2. Experimental procedures

2.1. Materials and preparation of calcium dialuminate

Three samples of bauxite from Haleo-Danielle Minim-Martap (Cameroon), D_{97}=0.1 mm, containing high amounts of gibbsite $Al(OH)_3$ [7,8,34,35] were weighed and mixed with lime (CaO) D_{97}=0.1 mm, (72% Al_2O_3, 28% CaO and water). The samples were labeled as CBX3, CBX55 and CBX8. The mixtures were molded, dried and heated for 2 h in an electric muffle furnace under ambient atmosphere at a heating ramp of 5 °C/mn up to 1550 °C. It must be noticed that the furnace we used leads to rather high cooling rate (15 °C/mn) from 1550 °C to 1000 °C; this means that high temperature phases are expected to be quenched. After heating, the products obtained were ground into powder and stored in polypropylene containers. XRD data were collected on a Philips PW 1710 diffractometer with CuKα λ_{Cu}=1.54056 Å radiation operated at 35 KV and 35 mA. The diffraction patterns were collected in the 2 theta range of 5–70°. Qualitative analysis of the phase composition of the powders was conducted using the PDF-2 release 2007 software. The average grain size distribution was performed using a Master Sizer 2000 granulometer. The density of the cement powder was determined using the Helium pycnometer method. The specific surface area of the cement powder was measured by the nitrogen adsorption BET method.

2.2. Characterization of cement based calcium dialuminate

The powders were mixed with an adequate amount of water (100 g of cement with 33 g of water), determined for each batch according to the cement CA14M-0,33 standard from Alcoa, and cast in a plastic mold with dimensions of 4 cm × 4 cm × 1 cm using a vibrating table at a frequency of 50 Hz and 3 min vibrating time. The hydrated cement was left in the mold for 48 h in a 100% relative humidity cabinet. The hydrated cement was then demolded and cured at 105 °C for 48 h at 100% relative humidity to accelerate the hydration of all the components in the cement. The bricks of the hydrated cement obtained were cut, ground into powder for phase identification by XRD using a Philips PW 1710 diffractometer with CuKα radiation as already described. Thermal analysis has been carried out with a DTA-TG LINSEIS (L81) coupled with a RIGAKU thermoflex; each experiment was done on 70–100 mg of hydrated cement under air with a heating ramp of

10 °C/min from room temperature to 1400 °C. A calcined alumina (1600 °C) reference material from PROLABO was used as a standard material. Scanning electron microscopy (SEM) has been carried out on a Philips XL30 equipment (10 KV) and at a resolution of × (500–7500) on the hydrated cement to determine the grain size and hydration process of the cement components. The elastic behavior of the materials involved in the perfect cohesive matrix was studied. An ultrasonic technique with transducers at a frequency of 10 MHz was used in transmission mode to measure the Young's modulus values based on Hooke's law. Dilatometric studies of hydrated and stabilized cements of dimensions 10 mm × 5 mm × 5 mm were performed at 10 °C/mn in air from room temperature up to 1500 °C with a ADAMEL, DI24 apparatus.

3. Results and discussions

3.1. Phase composition

X-ray diffraction patterns of the one stage sintered powders are shown in Fig. 1. Cements BX8 and BX55 present high intensities of CA_2 peaks. The secondary phases are not important as compared to the peaks presented by cement BX3 that are not attributed to CA_2. The additional phases (CT and TA) presented by CBX3 and the low alumina content in the raw bauxite can explain the relative low intensities of CA_2 peaks in the sample. In the three products, the XRD patterns indicate very high crystallinity of the CA_2 formed with no significant amorphous phase in the samples. The phase composition shown in Fig. 1 can be correlated to the bulk chemical composition shown in Table 1. BX55 and BX8 have 89.4 and 91.1 wt% of Al_2O_3 respectively and very low amounts of Fe_2O_3 (1.83 and 2.14 wt% respectively) and TiO_2 (1.4 and 1.13 wt% respectively) with respect to 80.26 wt% of Al_2O_3, 8.67 wt% Fe_2O_3 and 7.05 wt% of TiO_2 of BX3. The significant presence of Fe_2O_3 and TiO_2 in BX3 explains the presence of CT and TA as secondary phases in BX3. CA_2 and CA_6 are the readily thermodynamically stable compounds in the $CaO–Al_2O_3$ binary system with increasing refractoriness respectively [3–5]. The use of bauxite as raw materials allows ready transformation of the 1:4 mixture (CaO, $Al(OH)_3$) to $CaO \cdot 2Al_2O_3$ at 1550 °C. This is reported in the literature [8]. The formation of CaO-rich-phase and unreacted Al_2O_3 before the formation of $CaO \cdot 2Al_2O_3$ is due to the high reactivity of CaO with respect to Al_2O_3. The use of bauxite as an alumina source surely increases the reactivity of the system and allows rapid formation of the final product. The dehydroxylation of the bauxite results in the formation of high metastable alumina with high potential reactivity. Therefore the nature of raw source of alumina and the sintering process are significant when preparing the calcium dialuminate for refractory applications [6–12]. The mixture of CaO and Al_2O_3 generally used for the synthesis of CA_2 seems to be not as efficient as the direct activation of bauxite and CaO. The process used in this study avoids extensive development of various classes of calcium aluminate phases [5,6]. Generally, CA and CA_2 appeared simultaneously at the first stage of heating and the total conversion to CA_2 requires three or more firings with intermediate grinding and pelletizing. CA_2 was observed on the XRD patterns as mean crystalline phases and calcium titanate $CaO \cdot TiO_2$ (CT) perosvkite is produced during the sintering reactions as the secondary phase. The absence of the iron-rich phase even with the sample BX3 is explained by the ability of the Fe_2O_3 previously present in the bauxite sample to be incorporated in the crystalline structure. The possibility of the minimization of the ferritic mineral phase in the calcium alumina cement has been reported [3]. It was observed that during the crystallization process of calcium aluminate cement, Fe_2O_3 is firstly incorporated into the crystal lattice of CA and the rest of Fe_2O_3 crystallizes afterwards as the ferritic phase. It is worth stating that the absence of the ferritic mineral phase is due to the incorporation of the Fe_2O_3 in the lattice of CA_2. Trace compounds like MgO and SiO_2 present in the bauxite combined with alumina to form spinel ($MgO \cdot Al_2O_3$) and gehlenite ($SiO_2 \cdot 2CaO \cdot Al_2O_3$) phases; however, these compounds were not enough to be identified

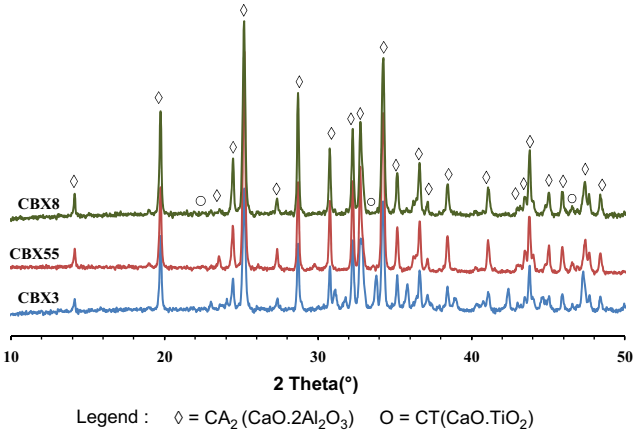

Fig. 1. XRD diffractogram of three powder cements (CBX8, CBX55 and CBX3).

Table 1
Specific area and density of powder cement.

Sample	Mass (g)	Adsorption (m^2)	Desorption (m^2)	Specific area (m^2/g)	Pygnometer density
Cement BX3	1.6078	0.83	1.15	0.72	3.17
Cement BX55	1.5203	0.35	1.29	0.85	2.95
Cement BX8	1.8655	1.00	1.32	0.80	2.98

by the XRD diffractogram. The absence of any peak belonging to $CaO \cdot Al_2O_3$, Al_2O_3 and CaO on our diffractogram suggests that transformation of the raw materials to CA_2 was almost completed. The sintering reaction equations can be summarized according to the XRD, DTA/DTG of the bauxites and the authors [32,33] as

$$Al(OH)_3 + Ca(OH)_2 \rightarrow CaO + 2Al_2O_3 \text{ (amorphous)} + 7H_2O \quad (1)$$

$$CaO + 2Al_2O_3 \text{ (amorphous)} \rightarrow CaAl_4O_7 \text{ (calcium dialuminate)} \quad (2)$$

It is well known that although the CA_2 has unique properties, the mineral suffers poor hydration capacity at ambient temperature. To overcome this challenge and optimize the reactivity of the refractory cements, they were cured at 105 °C with 100% humidity. The hydraulic activities of the products were studied using XRD, DTA and DTG. Fig. 2 shows the X-ray diffraction patterns of the hydrated cements. All the samples BX3 (1 0 5), BX55 (1 0 5) and BX8 (1 0 5) show one part of calcium dialuminate ($CaO \cdot 2Al_2O_3$), calcium titanate ($CaO \cdot TiO_2$) and hydrated components tricalcium aluminate hexahydrate ($3CaO \cdot Al_2O_3 \cdot 6H_2O$), associated with gibbsite ($Al_2O_3 \cdot 3H_2O$). The reaction of the hydration process is presented as follows [24]:

$$3CA_2 + 21H \rightarrow C_3AH_6 + 5AH_3$$

The XRD patterns of the hydrated samples of refractory cement show CA_2 with high intensity peaks, an increase in the amorphous phase and the appearance of new crystalline phases for all the three systems (Fig. 2). The presence of CA_2 on the hydrated matrices confirms the poor hydration ability of CA_2. In general the hydration of CA_2 is very slow and can take many days [1–6,30]. From the XRD patterns in Fig. 2, it is observed that there is a great reduction of CA_2 in sample BX3, while the peaks of CA_2 remain more prominent in samples BX8 and BX55. The reduction of the CA_2 phase which is common for all the samples is followed by the formation or increase of AH_3 and C_3AH_6 (Katoite). The amount of AH_3 in the samples is relatively low. It should be noted that the alumina phase is not observed in the cements (Figs. 1 and 2); however, the hydration may have allowed the formation of small amounts of residual alumina phases at the interlayer of the structure of the cement which were not enough to be identified by XRD. The absence of alumina phase in the refractory cement samples suggests the high degree of sintering achieved during the elaboration of the binders. Figs. 3–5 describe the behavior of the hydrated cement samples under thermal treatment. From ambient temperature up to 250 °C, the AH_3 loses its water leading to a total weight loss of 1 wt% for sample CBX3. The weight loss for samples CBX8 and CBX55 was 2 wt%. The first explanation for this behavior can come from the aluminum hydroxide content of the three cements. In fact the bauxites used for the sintering of the cements contained 80 wt% of alumina for CBX3 and 90 wt% for the BX8 and BX55. While the AH_3 phases tend to lose water, the significant CT phase in sample CBX3 does not allow weight loss. We can suggest that the higher the alumina content, the

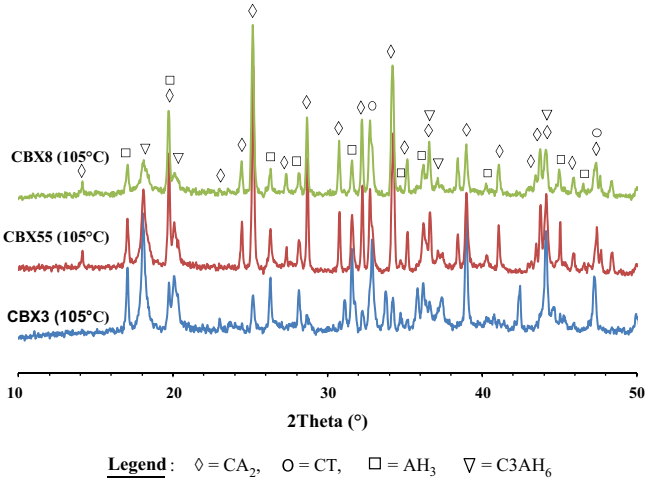

Fig. 2. XRD diffractogram of hydrated cement after stabilization at 105 °C for 48 h, W/C = 0.33.

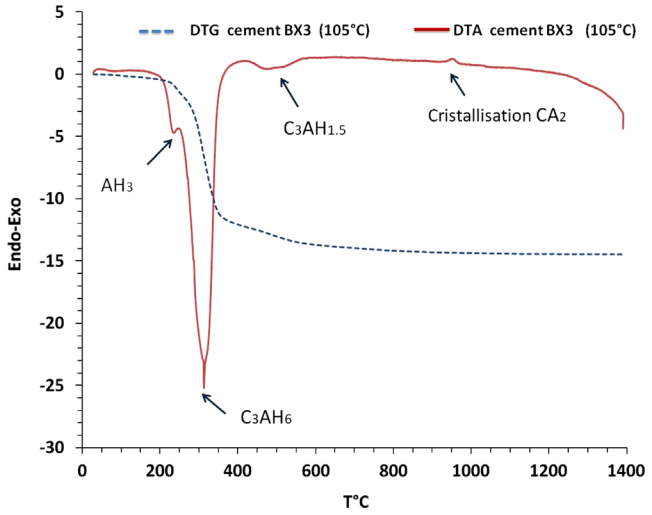

Fig. 3. DTA and DTG curves of cement BX3 after stabilization at 105 °C for 48 h.

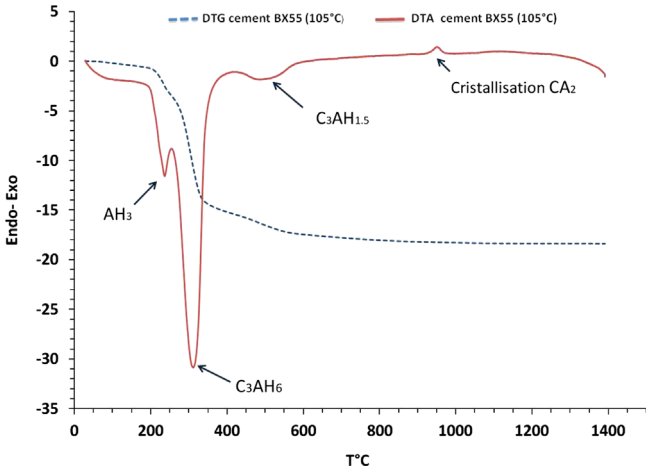

Fig. 4. DTA and DTG curves of cement BX55 after stabilization at 105 °C for 48 h.

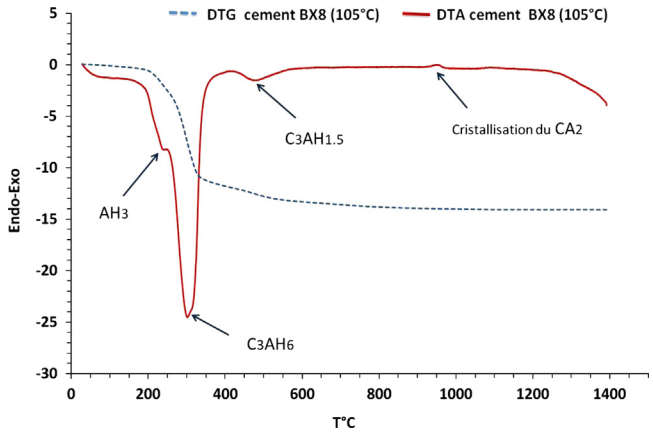

Fig. 5. DTA and DTG curves of cement BX8 after stabilization at 105 °C for 48 h.

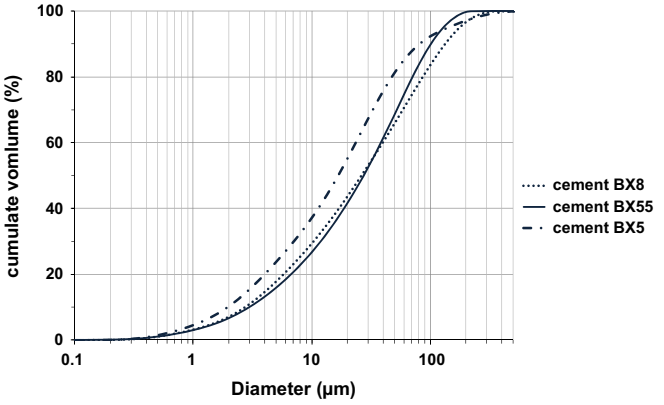

Fig. 6. Granulometry curves of BX55, BX8 and BX3 powder cement.

lower the residue of the non-sintered alumina and its rehydration in the cement matrices. However, the results of the DTA/TGA confirm the optimum transformation of the bauxite during sintering. Figs. 3–5 show evidence of the formation of C_3AH_6 as the principal phase in the refractory cements. Its decomposition at 300 °C releases significant amount of water: 14 wt% for CBX3 and CBX8 while CBX55 presented up to 17.5 wt% of water loss. From the XRD, the peaks intensity of CA_2 is low for the CBX3 sample and high with similar significance for CBX8 and CBX55: results that can be easily correlated to the bulk chemical composition of the three bauxites used. The fact that CBX3 and CBX8 present similar weight loss after the decomposition of C_3AH_6 is indicative of the non-uniformity of the hydration behavior of the three cements. CBX55 with a similar content of Al_2O_3 as CBX8 presented high hydration in regard to the total weight loss resulting from the decomposition of C_3AH_6. The presence of CT as from the TiO_2 and the incorporation of Fe_2O_3 in the crystalline phase during sintering have affected the structure of CA_2 matrices and their hydration capacities. The second endothermic peak at 500 °C is due to the thermal decomposition of $C_3AH_{1.5}$. Even though this appears not as significant as the decomposition at 300–310 °C, one can conclude on the partial decomposition of C_3AH_6 at around 300 °C and some transitional phases that see their total decomposition take place only at 500 °C. The decomposition of the C_3AH_6 can be described with two sequences of reactions from DTA/TGA and the authors [25]:

$$\text{At } 310\ ^\circ\text{C} \quad C_3AH_6 \rightarrow C_3AH_{3/2} + 9/2H$$

$$\text{And at } 500\ ^\circ\text{C} \quad C_3AH_{3/2} \rightarrow C_3A$$

The compound $Ca_3Al_2O_6$ remains a metastable compound that will reorganize itself with free alumina from gibbsite to form stable CA_2 at 950–970 °C. The matrix with CA_2 remains stable up to the densification at temperature beyond 1300 °C. For CBX3, the densification took place before 1300 °C. The presence of CT as well as the incorporation of iron in the structure of the CA_2 phase has a large effect on the extent of densification. The grain size is then increased and the microstructure is then stabilized again with hydration as already indicated above (Figs. 3–5). Kumar et al. [6] described calcium dialuminate with particle size under 100 µm. In this study, about 87 vol% of the particles of the cement CBX8 have the particle size under 90 vol% of particles of CBX55 and 93 vol% of CBX3 have size under 100 µm (Fig. 6). The grains growth in the CA_2 cement and the development of highly dense matrices is essential to explain the resistance to hydration. In the final products from CBX8, CBX3 and CBX55, the crystal size of CA_2 and the secondary phases is controlled by the temperature and the impurities content. Although the CA_2 is known for its low rate of hydration, the use of curing at 105 °C and the porosity of the microstructure would have contributed to some improvement of the process of hydration in comparison to what is described in literature [20–24,30]. Singh and Majundar [3] have postulated that hydration of CA_2 cements starts at an earlier time when a quantity of granulated blast furnace slag is added. Parker et al. [23] found that the hydration of pure CA_2 is not efficient even after 24 h of curing when the temperature is maintained at 20 °C. Hence unlike the coarsening of the cement particles, the use of bauxites described in this work can find some advantages for their applications where temperatures beyond 1300–1400 °C are not required. For very high temperatures, only CBX55 was found to be suitable as an effective refractory cement. The dilatometric curves of Fig. 7 show a shrinkage of 0.8% for CBX8 and CBX55 and 1% for CBX3 when the temperature is 310 °C. The shrinkage here corresponds to the dehydration of AH_3 and C_3AH_6. The departure of water left some porosity at the origin of shrinkage. However, in spite of the importance of dehydration (Figs. 3–5), the energy available at this temperature was not enough to make a significant volume contraction. Another slight contraction of volume is observed between 950 and 1000 °C for all the three samples. Making reference to the differential thermal analysis curves, the shrinkage can be due to crystallization. The transformation of a hydrated phase to an anhydrous one results in a volume contraction. At this point the total shrinkage is 1% for CBX3 and CBX55 but relatively high for CBX8 (2%). At 1300 °C, densification initiates with significant volume contraction. At this temperature, the energy available is sufficient to eliminate voids available in the

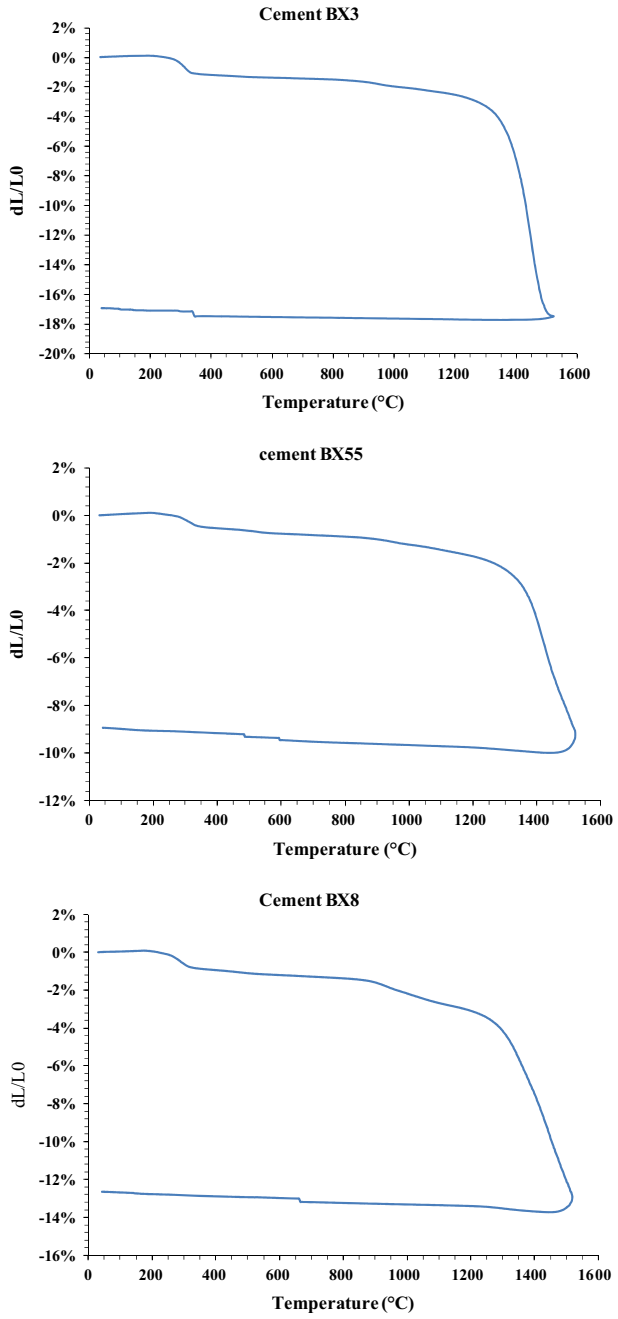

Fig. 7. Dilatometric curves of hydrated cement BX3, BX8 and BX55 after stabilization at 105 °C.

matrixes. Here once again the difference of structural imperfection between the samples due to the impurities is traducing the difference in densification. At 1500 °C, CBX55 presents only 9% of shrinkage while CBX8 and CBX3 presented 12.4 and 17% of shrinkage respectively Fig. 7.

3.2. Densification, Young's modulus behavior and microstructure

The densities of the CA_2 matrices are 2.95, 2.98 and 3.17 g/cm^3 respectively for CBX55, CBX8 and CBX3. The relatively high value of density (Table 1) of sample BX3 compared to BX8 and BX55 can be justified by the bulk chemical composition of the raw materials used for this study. The presence of TiO_2+Fe_2O_3 (15.7 wt%) (Table 2) in this sample explains the formation of the CT phase; the coarsening of the grains of CA_2 is due to the incorporation of iron in their structure and earlier densification described with DTA/TGA (Figs. 3–5) and dilatometry (Fig. 7). The high density of CBX3 as well as the coarsening of grains presented gives rise to lower specific area (0.72 m^2/g) with respect to 0.85 and 0.80 m^2/g respectively of CBX8 and CBX55. This trend also follows the desorption and absorption behavior of the three cements. The variation of the total porosity presented could explain the latter (Table 1). In Fig. 8, it is observed that sample BX3 with high impurities content displayed higher porosity (25 vol%) and a lower value of Young's modulus.

The increase of Young's modulus of sintered cement is due to the excess CA_2 refractory compound than the conventional cement that contains majority of CA (Table 3), which is less refractory and not more rigid. A study of the phase diagram of the binary CaO–Al_2O_3 system indicates that the cement contains 26–32 wt% CaO and has a mixture of CA and CA_2, where CA has a lower modulus of elasticity and a lower thermal expansion coefficient than CA_2. Fig. 8 also demonstrates Young's modulus of cement with the decreasing porosity.

The same value of porosity is observed in CBX3 and CBX8 with different values of Young's modulus. This difference reveals that Young's modulus of hydrated bodies increases with decreasing impurities like Fe, Ti, and Si in the cement. The high value of Young's modulus 39.4 GPa with a porosity of 11.63% has been observed from cement BX55. From the authors [9] the higher magnitude of Young's modulus is believed to be caused mainly by the higher CaO content of the stabilised cement paste and the larger holding time (5 h) at temperature 1500 °C, while in this work, the presence of CA_2 is the only phase that gives much higher Young's modulus than the presence of a mixture of CA and CA_2 which consequently demonstrates that the probability of the setup of bond linkage between CA_2 and CA_2 grains in the matrix is higher than CA and CA in the matrix. Sample BX8 presents a similar value of porosity but with high Young's modulus value. The value of porosity of BX55 was 11.63 vol%, half of the total porosity presented by BX3 and BX8. The Young modulus values of 35.5, 38 and 39.4 GPa could be easily correlated to the alumina content of the raw bauxites used. Moreover, these values were inversely proportional to the impurities content (mainly Fe_2O_3 and TiO_2). It was concluded that the purity of the bauxite reduces the rate of grain growth during sintering. From Fig. 6, it can be observed that sample BX55 presents a finer grains size. Lower amounts of impurities in this sample would have enhanced the development of smaller size of grains and hence improvement in the packing process with consequent reduction of intergranular voids. This packing process allows an increase of the Young modulus with respect to sample BX3 where impurities would have increased the porosity and thereby reduced the Young modulus. The fact that BX8 and BX3 showed similar porosity (25 vol%) and have different values of Young's modulus is still linked to the purity

Table 2
Constituents of alumina cement.

Sample	SiO_2	Al_2O_3	CaO	MgO	Na_2O	K_2O	Fe_2O_3	TiO_2	Total
BX3	0.52	80.26	0.04	0.08	0.073	0.014	8.67	7.05	**96.73**
BX55	Nd	89.4	0.018	Nd	Nd	Nd	1.83	1.4	**92.6**
BX8	0.65	91.10	0.00	0.01	0.000	0.050	2.14	1.13	**95.08**
Lime	Nd	Nd	95.58	1.3	Nd	Nd	Nd	Nd	**97.1**

Table 3
Identification of the phases present in refractory cements.

Temperature of hydrated phase	Cement made from bauxite (28% CaO, 72% Al_2O_3)
$T^\circ < 110 \pm 5\ ^\circ C$	CA_2, CT, C_3AH_6, AH_3
$110 \pm 5 < T < 500\ ^\circ C$	CA_2, CT, $C_3AH_{1.5}$
$500 < T < 950\ ^\circ C$	Dehydroxylation of $C_3AH_{1.5}$
$T > 950\ ^\circ C$	Anhydrous phases CA_2, A, CT

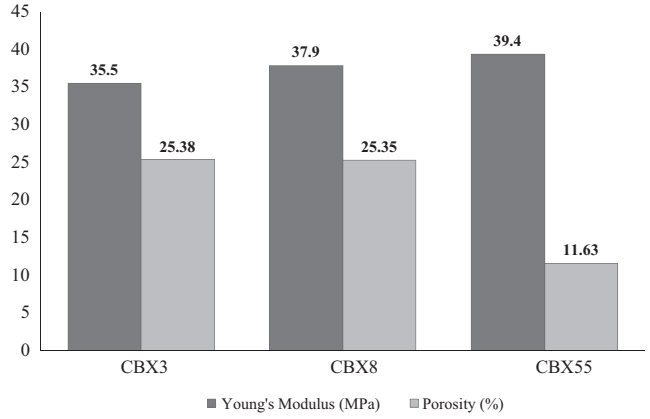

Fig. 8. Young's modulus and porosity of different cements after stabilization at 105 °C.

of the raw samples of bauxites used. Globally, the value of Young's modulus presented by the present samples of refractory cements is relatively high with respect to the Young modulus of CA_2 matrices available in the literature [14–25]. In fact most authors generally describe CA_2 with additional CA or some other secondary phases. Moreover much of the pure CA_2 available in the literature is amorphous or semi-crystalline [26,27], a situation that is absolutely not favorable for their mechanical behavior. The sintering method proposed here is of greater advantage to the design of refractory cements with upgrade properties [28,29].

Fig. 9 shows the micrographs of the calcined bauxites treated at 1500 °C as granulate. Specimen BX3 seems to contain the highest amount of titanium oxide as evident by the white color observed compared to BX8 and BX55. Fig. 10 shows the grains size of the cement and the pores exhibited during the hydration of cement. The grains sizes of cement CBX55 are better grown than CBX3 and CBX8. In fact this result is in agreement with the variation of the porosity assessed using the density method (Table 1). The pore size in BX55 is very fine and can explain the relatively low content of impurities which did not hinder the high compactness of the sample. In Fig. 10, high magnification of micrographs allows the observation of the phase distribution in the matrices of refractory cements. Samples BX3 and BX8 present more heterogeneity and dispersion in the phases content. These samples with relatively high impurities have microstructure different from that of BX55. Even though it was not evident to identify some minor phases in the cements using XRD, it should be noted that 0.52 wt% and 0. 65 wt% of SiO_2 are present in BX3 and BX8 respectively. This silica most probably amorphous will tend to favor the heterogeneous densification and dispersion of newly formed phases. 7.05 wt%, 1.4 wt% and 1.13 wt% of TiO_2 are present in BX3, BX55 and BX8 respectively. In the same order, 8.67 wt%, 1.83 wt% and 2.14 wt% of Fe_2O_3 were identified in the samples of raw materials for the refractory cements. The effects of TiO_2 and Fe_2O_3 on the microstructure are the formation of the CT phases with more light in the micrographs with content that follow the amount of iron and titanium in the raw samples of bauxite. The authors [3,4,13] showed the important role played by iron in enhancing the crystallization of Calcium hexaluminate cements. They demonstrated the progressive shift to lower temperatures of the formation of hexaluminate phases with the increase in iron content. The presence of iron could be attributed to the substitution of Al^{3+} with Fe^{3+}. This substitution was at the origin of the expansion of a unit cell with increasing Fe^{3+} content. In Fig. 6, we observed the difference in the coarsening of grains with CBX55 presenting the tinier particles. The coarsening of the cement particles followed by the difference of the iron content means that our hypothesis of the incorporation of iron in the structure of CA_2 is in agreement with the phase evolution and microstructure. Fig. 10 shows the significance of this difference of TiO_2 and Fe_2O_3 content on the crystallization, grain growth and grains boundaries. Fig. 10a shows the CT phase and some amorphous structure in the grains boundaries, an indication of the origin of heterogeneity of the distribution of CA_2 phase in the matrix. These amorphous phases were at the origin of the minor liquid

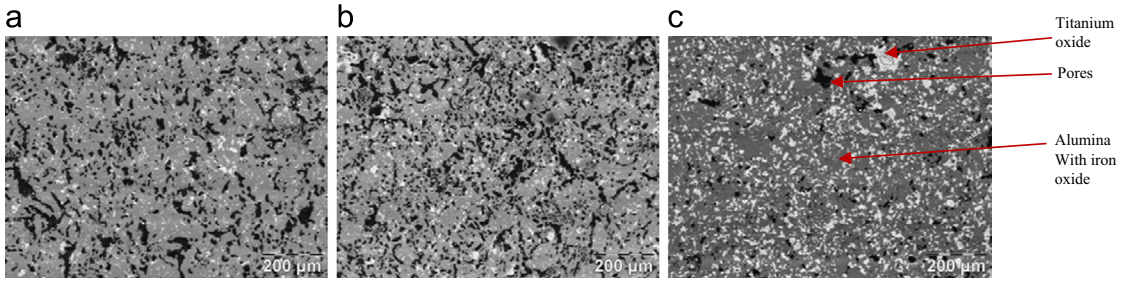

Fig. 9. Different micrographs of bauxite granulate BX8, BX55 and BX3 on back scattered electrons (BSE) after being heated at 1500 °C.

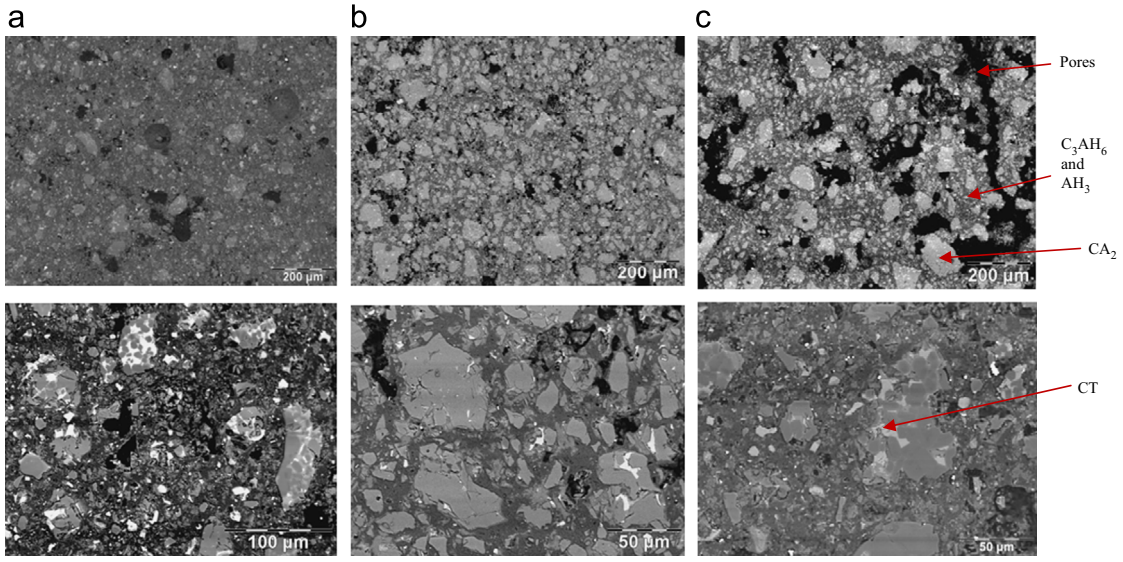

Fig. 10. Different micrographs of hydrated cement CBX3, CBX55 and CBX8 on back scattered electrons (BSE) after stabilization at 105 °C.

phase which can easily explain the round shape of some of the pores identified in the CBX3 samples during the SEM investigations (Fig. 9). In the literature the liquid phase has been identified to enhance the grain growth phenomenon which could be the case here as we can observe in Fig. 11.

Figs. 10 and 11 show the SEM micrographs of hydrated cement after stabilization at 105 °C. These micrographs show that different locations and magnifications networks of CA_2 plates and $CaO \cdot TiO_2$ could be observed in all samples in back scattered electrons (BSE) forming the matrix of this microstructure. The bonding role is favored by C_3AH_6 and AH_3 interlocking the hydrated product. The hydrated phase surrounds the grain of CA_2 and sets up the bond linkage between CA_2 and CA_2 in the bonding matrix by C_3AH_6 and AH_3; this bonding matrix is believed to cause the increase in Young's Modulus in the cement.

4. Discussion and conclusions

4.1. Surface charge of cement particles

Surface charge of aluminous cement particles is involved in the hydration mechanisms of calcium aluminate cement [31]. The sign of the surface charge of starting cement particles can be estimated. One approach can be considered by statistical representation of the charges on the surface of the cement grains to estimate the electric state of the surface in the case of major component of the calcium aluminate cement (CA, $CaO \cdot Al_2O_3$) [31]; by denoting $\sigma+$ and $\sigma-$ as the surface charges of the positive and negative sites for this component it yields from Fig. 12

$$\frac{\sigma+}{\sigma-} = \frac{(Ca^{2+})\text{surface projection} + 2(Al^{3+})\text{surface projection}}{4(O^{2-})\text{surface projection}}$$

where (Ca^{2+}) surface projection, (Al^{3+}) surface projection and (O^{2-}) surface projection are equal to πr^2 ion radius associated with each ion, in which the ionic radius of each element is known, namely 1.35 Å for oxygen, 1.05 Å for calcium and 0.5 Å for aluminum. For CA $(\sigma+/\sigma-) = 0.22$ and for CA_2 $(\sigma+/\sigma-) = 0.16$. The surface charge of cement is negative; although this approach gives interesting results, it is somehow too simplistic because it assumes that all surfaces have the same atomic arrangement and that the surface of the grains has the same chemical composition as that of the bulk. The strongest negative charge of calcium dialuminate cements improves their resistance to the corrosive effects of certain acids and industrial wastes. They can be used to resist corrosion down to a pH of about 3.5–4.0 depending on the

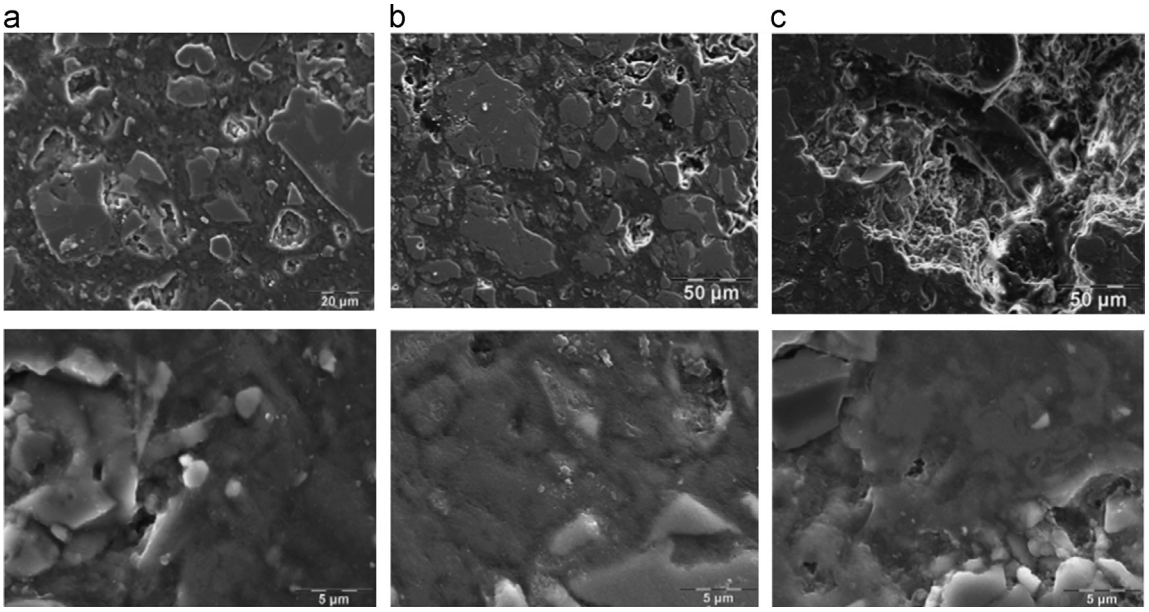

Fig. 11. Different micrographs of hydrated cement CBX3, CBX55 and CBX8 after stabilization at 105 °C.

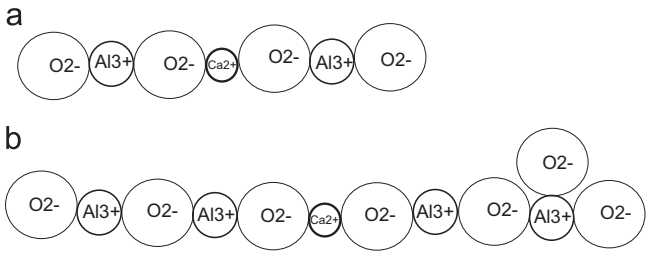

Fig. 12. Statistical representation of the distribution of the surface charges for anhydrous grain of $CaO \cdot Al_2O_3$ (a) and $CaO \cdot 2Al_2O_3$ (b).

type of acid, temperature, length of exposure, frequency of washing and other factors. This makes the concretes suitable for use in such corrosive environments as wineries, tanneries, sugar refineries, breweries, bakeries, dairies, fisheries and food processing plants. These cements are also resistant to alkalis up to a pH of 12, with the exception of alkali hydroxides. The cement made will be used for making concrete that is suitable for exposure to sulfate ground water and seawater.

4.2. Mechanism and kinetics of $CaAl_4O_7$ formation at 1550 °C

Activation energies (E_a) for the growth crystal and diffusion processes are presented. It is seen that the mechanism operates for CA_2 crystallite growth from solid-state reactions between crystallite CaO and Al_2O_3 [32]; the high E_a for Al diffusion in Al_2O_3 (477 KJ/mol) versus the lower E_a for Ca in CaO (142–268 KJ/mol) indicates that Ca diffuses into Al_2O_3 to form $CaAl_4O_7$. This explains why the E_a for conventional $CaAl_4O_7$ formation is comparable with the E_a for Ca diffusion in CaO. The mechanism for solid state reaction between crystalline CaO and Al_2O_3 to form $CaAl_4O_7$ occurs at the $CaAl_2O_4$–Al_2O_3 interface and necessitates the diffusion of Ca through the product phase toward Al_2O_3. The growth kinetic exponent, n, for this type of reaction is considered to be 2. The kinetics of isothermal growth are described by the phenomenological rate equation:

$$G^n - G_0^n = K_0 t \exp(-E_a/RT)$$

where n is the growth kinetic exponent, G is the average crystallite size at time t, G_0 is the nucleus size and K_0 is the temperature independent rate constant that includes frequency and geometric factors as well as entropy terms. E_a is the activation energy for the growth process; R and T are the universal gas constant and the absolute temperature respectively. Taking the time derivation of G for constant n gives the reaction rate q. The activation energy E_a can be then determined from the plot of $\ln(q)$ versus $1/T$; $\ln(q) = \ln K_0 - (E_a/R)(1/T)$; the activation energy of $CaAl_4O_7$ is calculated and we obtain about 140 KJ/mol.

The three precursors we used for this study could be classified as iron+titanium rich bauxite (BX3) and pure alumina hydroxide based bauxite (BX55). The sample BX8 is here considered as intermediate between both. The sample with impurities (iron+titanium) results in the formation of coarser grains of CA_2 with additional CT (Figs. 1 and 2). The sample of cement from this sample showed abnormal grain growth and grain boundaries in the microstructure. The growing of grains may be explained by the incorporation (substitution) of iron in the structure of CA_2. It was demonstrated that this incorporation of iron ions gives rise to a drop in the sintering temperature. Iron and titanium impurities may segregate to the grain boundaries or form secondary phase at the grain boundaries (Fig. 11). The mobility of grains at grain boundaries could then be modified with significant modification of the porosity and mechanical properties (Figs. 8 and 11). Even though in the case of BX8 these secondary phases were not enough to be identified by XRD patterns, it was agreed that it presented relatively wet grain boundaries due to the presence

of the amorphous phase. For sample BX55, $Al(OH)_3$ and $Ca(OH)_2$ were pure enough, avoiding intermediate phases between CA_2 grains. During sintering, the contact between grains allows uniform diffusion between alumina and calcium oxide with regular and homogeneous matrix. We demonstrated that the direct process of synthesis of CA_2 with one stage heating by solid state sintering is possible and raw bauxite from Cameroon with their Fe_2O_3 and TiO_2 content are suitable for the production of CA_2 matrices where very high temperature is not required. Additionally, BX8 and BX55 represent the cases of the success of the process when compared to the conventional solid state route with pure Al_2O_3. This process may be economically sustainable in energy consumption. The absence of silica in the bauxite could extend the chances of application to linings of such a large scale installation as steel ladles and cement kilns. However the kinetics of the CA_2 phase at ambient temperatures would still need to be evaluated.

References

[1] S. Jonas, F Nadachowski, A new non-silicate refractory of low thermal expansion, Ceramics International 24 (1998) 211–216.

[2] Kenneth J.D. Jadambaa Temuujin, Tsedev MacKenzie, Banzar Jadambaa, Budjav Namjildorj, Mark E. Olziiburen, Smith, Paul Angerer, Effect of mechanochemical treatment on the synthesis of calcium dialuminate, Journal of Materials Chemistry 10 (2000) 1019–1023.

[3] B Singh, A.J. Majumdar, The hydration of calcium dialuminate and its mixtures containing slag, Cement and Concrete Research 22 (6) (1992) 1019–1026.

[4] S. Jonas, F. Nadachowskia, D. Szwagierczak, Low thermal expansion refractory composites based on $CaAl_4O_7$, Ceramics International 25 (1999) 77–84.

[5] M.F. Zawrah, N.M. Khalil, Synthesis and characterization of calcium aluminate nanoceramics for new applications, Ceramics International 33 (2007) 1419–1425.

[6] Sanjay Kumar, A. Bandopadhyay, T.C. Alex, Rakesh Kumar, Influence of mechanical activation on the synthesis and hydraulic activity of calcium dialuminate, Ceramics International 32 (2006) 555–560.

[7] Omer Arioz, Effects of elevated temperatures on properties of concrete, Fire Safety Journal 42 (2007) 516–522.

[8] Cristina Dominguez, Jerome Chevalier, Raman Torrecillons, Gilbert Fantazzi, Microstructure development in calcium hexaluminate, Journal of the European Ceramic Society 21 (2001) 381–387.

[9] F.M. Lea, in: Peter C. Hewlett (Ed.), Lea's Chemistry of Cement and Concrete, fourth ed., Arnold, 1988.

[10] K Fujji, W Kondo, H Ueno, Kinetics of hydration of monocalcium aluminate, Journal of American Ceramic Society 69 (4) (1986) 361–364.

[11] Mohammad Reza* Nilforoushan, Nasrien Talebiaan, The hydration products of a refractory calcium aluminate cement at low temperatures, Iranian Journal of Chemistry and Chemical Engineering 26 (2) (2007).

[12] F. Simonin, C. Olagnon, S. Maximilien, G. Fantozzi, Room temperature quasi-brittle behavior of an aluminous refractory concrete after firing, Journal of the European Ceramic Society 22 (2002) 165–172.

[13] M.A. Gulgun, O.O. Popoola, W.M. Krriven, Chemical synthesis and characterization of calcium aluminate powders, Journal of American Ceramic Society 77 (2) (1994) 531–539.

[14] Y.C. Ko, C.F. Chan, Effect of spinel content on hot strength of alumina–spinel castables in the temperature range 1000–1500 °C, Journal of European Ceramic Society 19 (1999) 2633–2639.

[15] E. Nonnet, N. Lequeux, P. Boch, Elastic properties of high alumina cement castables from room temperature to 1600 °C, Journal of European Ceramic Society 19 (1999) 1575–1583.

[16] W. Kurdowski, Poradnik technologa przemyslu cementowego, Wydawnictwo Arkady, Warszawa128–131.

[17] M. Jung, Hydraulic Properties of High-alumina Cements, in: International Symposium on Refractory Concretes, Czechoslovakia, 1971.

[18] W. Gessner, S. Moehmel, Th. A Bier, Effects of the alumina quality on hydration and thermal behaviour of calcium aluminate/alumina mixes, in: Proceedings of the International Symposium, Conference on Calcium Aluminate Cements, R.J. Mangabhai (Ed.), Londres, 1990.

[19] S. Moehmel, W. Gessner, D. Müller, Th. Bier, The behavior of CA/CA_2 cements during hydration and thermal treatment, in: Proceedings of the 5th UNITECR, Nouvelle Orléans, USA, vol. 3, 1997, pp. 1273–1282.

[20] H.J. Kuzel, Uber die orientierte entwässerung von tricalcium aluminate hydrate $3CaO \cdot Al_2O_3.6H_2O$, Neues Jahrbuch für Mineralogie Monatshefe (1969) 397–403.

[21] M.C. Ball, The thermal dehydroxylation of C_3AH_6, Cement and Concrete Research 6 (1976) 419–420.

[22] H. Marzagui, T. Cutard, Characterization of microstructural evolutions in refractory castables by in situ high temperature ESEM, Journal of Materials Processing Technology 155–156 (2004) 1474–1481.

[23] R.N. Edmonds, A.J. Majumdar, The hydration of mono calcium aluminate at different temperatures, Cement and Concrete Research 18 (1988) 311–320.

[24] F Nazaret, H Maragui, T Cutard, Influence of the mechanical behavior specificities of damaged refractory castables on the Young's modulus determination, Journal of the European Ceramic Society 26 (2006) 1429–1438.

[25] Jean Michel Auvray, Elaboration et caractérisation à haute température de bétons réfractaires à base d'alumine spinelle (Thèse de Doctorat), Université de Limoges, 2003 (in French).

[26] V.K. Singh, U.K. Mandal, Kinetics study of the thermal synthesis of calcium aluminate above 1400 °C, Transactions and Journal of the British Ceramic Society 81 (4) (1982) 112–113.

[27] G.B. Palmer, G Baker, Specimen size effect on fracture toughness for a low cement refractory, Theoretical and Applied Fracture Mechanics 22 (1995) 51–61.

[28] M Uberoi, S.H. Risbud, Processing of amorphous calcium aluminate powders at < 900 °C, Journal of American Society 73 (56) (1990) 1768–1770.

[29] M.F. Zawrah, N.M. Khalil, Utilization of Egyptian industrial waste materials in manufacture of refractory cement, British Ceramic Transactions 101 (5) (2002).

[30] Ömer Ariöz, Gökhan Arslan, Mustafa Tuncan, Serkan Kivrak, Web-based quality control of ready mixed concrete, Building and Environment 42 (2007) 1465–1470.

[31] Mustafa Tuncan, Omer Arioz, Kambiz Ramyar, Bekir Karasu, Assessing concrete strength by means of small diameter cores, Construction and Building Materials 22 (5) (1988) 981–988.

[32] A. Smith, Y. el Hafiane, J.P Bonnet, Role of small addition of acetic acid on the setting behavior and on the microstructure of a calcium aluminate cement, Journal of the American Ceramic Society 88 (8) (2005) 2079–2084.

[33] A. Mehmet, Oludele O. Gülgün, Popoola, Waltraud M. Kriven, Chemical synthesis and characterization of Calcium Aluminate powders, Journal of the American Ceramic Society 77 (2) (1994) 531–539.

[34] A.B. Tchamba, U.C. Melo, E. Kamseu, R. Yongue, D. Njopwouo, Thermal and sintering behavior of bauxite from Haleo-Danielle, Minim-Martap (Cameroun), Industrial Ceramic 30 (1) (2010) 6p.

[35] A.B. Tchamba, R. Yongue, U.C. Melo, E. Kamseu, D Njoya, D. Njopwouo, Caractérisation de la bauxite de Haléo-Danielle en vue de son utilisation industrielle dans les matériaux à haute teneur en alumine, Silicate Industrials 73 (5–6) (2008) 77–84.